FIBRILPAINTS AS A TOOL TO BIND AND MODULATE HUNTINGTIN AMYLOIDS

Françoise A. Dekker[1, 2, 3], Emile van Weert[4], Alfred C.O. Vertegaal[4], Assaf Friedler[5], *, Stefan G. D. Rüdiger[1, 2, 3, *]

[1] Protein Chemistry of Disease, Department of Chemistry, Utrecht University, Padualaan 8, 3584CH Utrecht, The Netherlands.

[2] Cellular Protein Chemistry, Bijvoet Center for Biomolecular Research, Utrecht University, Padualaan 8, 3584CH Utrecht, The Netherlands.

[3] Science for Life, Utrecht University, Padualaan 8, 3584CH Utrecht, The Netherlands.

[4] Department of Cell and Chemical Biology, Leiden University Medical Center, Leiden, The Netherlands

[5] Institute of Chemistry, The Hebrew University of Jerusalem, Edmond J. Safra Campus at Givat Ram, Jerusalem 9190401, Israel.

* Corresponding author

Running title

Amyloid binder

Abstract

Huntington's disease (HD) is caused by expansion of a polyglutamine tract in the huntingtin (HTT) protein, leading to aggregation of the exon 1 fragment (HttEx1) into amyloid fibrils. HttEx1 forms one of the lowest-complexity amyloid cores known, its fibril core consists of a single amino acid, glutamine. With emerging therapies improving patients' prospects by silencing expression of HTT, tools to monitor HttEx1 aggregation become essential for timely intervention and next-generation therapeutics. Here, we show that the peptide FibrilPaint1 selectively binds HttEx1Q44 fibrils without interacting with monomeric protein, allowing to measure and trace HttEx1 amyloid fibrils. Using the FibrilRuler assay, we tracked fibril formation from early species to larger clustered assemblies. The non-fluorescent variant, FibrilPaint20, was used to recruit the E3 ubiquitin ligase CHIP to HttEx1 fibrils, enabling site-specific ubiquitin tagging. However, unlike Tau fibrils, ubiquitinated HttEx1 fibrils resisted proteasomal degradation. This reveals a fundamental difference in how amyloids with extremely low–complexity cores respond to cellular clearance machinery. Together, our findings establish the FibrilPaint peptide family as a toolset for the detection and molecular targeting of amyloids, providing new opportunities to study protein aggregation and act as building blocks for future diagnostic and therapeutic strategies in neurodegenerative diseases.

Keywords

Huntingtin, FibrilPaint, Protein aggregation, Flow Induced Dispersion Analysis (FIDA), amyloid fibrils

Highlights

- FibrilPaint1 selectively binds HttEx1Q44 amyloid fibrils and monitors fibril growth using the hydrodynamic radius (FibrilRuler).
- FibrilPaint20 recruits the E3 ligase CHIP to Htt fibrils, enabling ubiquitination.
- Despite successful ubiquitination, Htt fibrils resist proteasomal degradation in vitro, highlighting structural barriers.
- FibrilPaint peptides provide a modular platform for studying and functionally engaging amyloids, with potential applications in diagnostics and targeted therapies for neurodegenerative diseases.

Graphical abstract

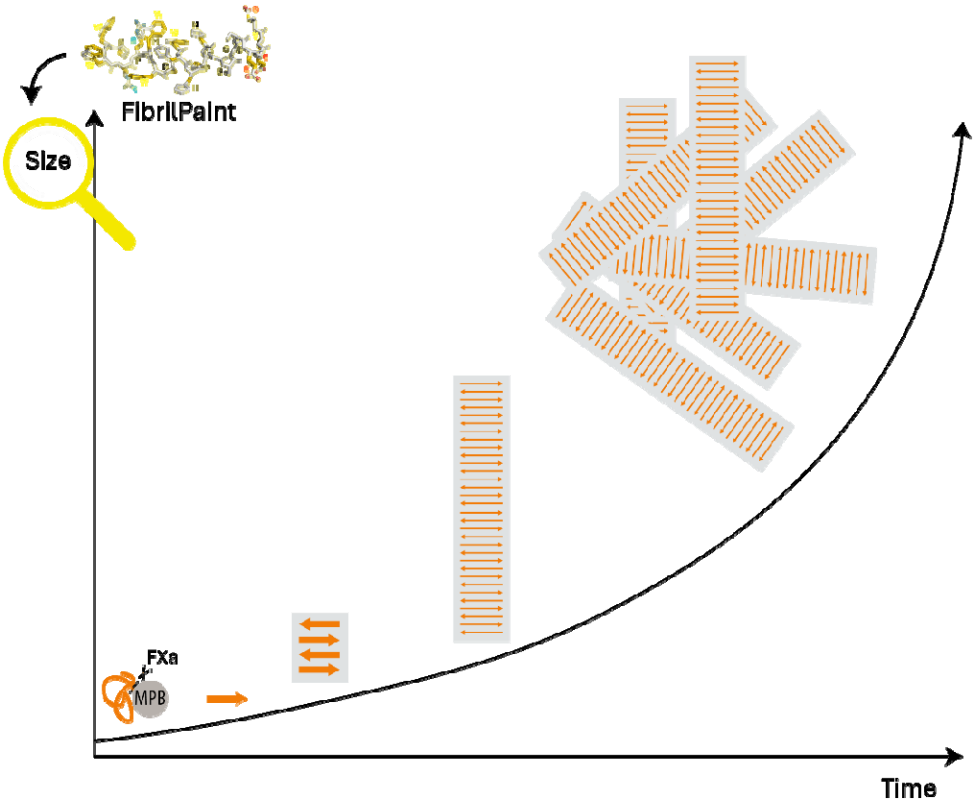

Graphical abstract – **The FibrilRuler Test: FibrilPaint enables measurement of Huntingtin fibril size during aggregation.** Following removal of the protective MBP tag by Factor Xa, a short lag phase precedes rapid fibril elongation. Subsequent fibril clustering further accelerates growth, leading to exponential increases in aggregate size.

Introduction

Huntington's disease (HD) is an autosomal dominant neurodegenerative disorder characterized by progressive tissue loss in the neocortex and striatum, leading to motor, cognitive, and psychiatric symptoms [1, 2]. It affects approximately 6 - 9 individuals per 100,000 in the Western world [3]. The disease is caused by an expanded CAG trinucleotide repeat in the Huntingtin (HTT) gene, which encodes an abnormally long polyglutamine (polyQ) tract in exon 1 of the huntingtin protein (Htt) [1, 4-7]. A polyQ stretch exceeding 35 glutamines is pathogenic, and disease onset and severity correlate with its length [2, 8].

mHttEx1 forms amyloid fibrils that accumulate as large intracellular inclusions and resist cellular clearance mechanisms [9, 10]. Structurally, the HttEx1 fragment consists of three domains: an N-terminal region, the polyQ tract, and a C-terminal segment. The polyQ core forms the amyloid backbone, assembling into antiparallel, non-twisting β-sheets [11, 12]. The N-terminal region initiates intermolecular contact, and together with the C-terminus, forms a dynamic "fuzzy coat" that surrounds the fibril core [12-14]. This stands in contrast to other disease-associated amyloids, such as Tau, α-synuclein, and Aβ, which possess chemically diverse, multi-residue cores capable of twisting and forming multiple conformations [12, 15].

Therapeutic strategies are emerging to target or prevent the aggregation process [16-18]. Notably, uniQure recently reported encouraging results from two Phase I/II clinical trials (NCT04120493, NCT05430117) using AMT-130, a gene therapy designed to silence HTT expression [19]. High-dose treatment resulted in up to 75% slowing of clinical decline in early-manifest HD patients, alongside reductions in cerebrospinal fluid neurofilament light (NfL), a marker of neurodegeneration [19]. These findings represent a breakthrough and provide strong support for therapeutic approaches that prevent or delay amyloid formation. However, gene silencing alone does not eliminate pre-existing aggregates, underscoring the need for complementary strategies and tools to track residual pathology.

To this end, we need reliable methods for detecting and quantifying mHttEx1 species [20-22]. Genetic testing and symptom presentation are effective for diagnosis of HD, and monitoring can supported by indirect biomarkers such as NfL levels or MRI-based measures of brain atrophy [23, 24]. While novel PET tracers like [^11C]CHDI-180R shows promise for imaging mHTT aggregates, they are still limited by high intersubject variability and low signal-to-background ratios [25, 26]. So, huntingtin pathology remains undetectable in patients. Chemically, this poses an interesting challenge, because the polyQ core lacks the chemical diversity typically required for selective molecular recognition [12, 15].

We previously developed FibrilPaints: modular peptides that selectively bind amyloid fibrils and can be functionalized for detection or enzymatic recruitment of the ubiquitin system [27-29]. Although all variants affected Tau aggregation kinetics, only FibrilPaint1 bound with sufficient affinity to enable fibril size quantification by Flow-Induced Dispersion Analysis (FIDA), a setup we termed the FibrilRuler test [27]. In this study, we examined their effect on Huntingtin Exon 1 with 44 glutamines (HttEx1Q44), the fragment that aggregates in HD. We also explore targeted modification of fibrils via FP20-mediated recruitment of the ubiquitination machinery. Our approach presents a modular toolkit for studying Htt aggregation.

Results

FibrilPaint1 specifically binds HttEx1Q44 fibrils, not monomers

We first assessed the effect of FibrilPaint addition on HttEx1 aggregation, both to establish a baseline for binding detection and to enable direct comparison with our earlier findings in Tau [27]. Aggregation was initiated by cleavage of the N-terminal maltose-binding protein (MBP) tag using Factor Xa (FXa), which triggered fibril formation **(Fig. 1A)**. Aggregation kinetics were monitored by Thioflavin T (ThT) fluorescence, an established reporter of β-sheet–rich amyloid structures [30]. FibrilPaint1–4 were added at final concentrations of 0.2, 1, and 2 µM, and ThT fluorescence was recorded over 10 h. All peptides reduced the final ThT plateau of 20 µM HttEx1Q44 aggregation in a concentration-dependent manner, indicating interaction with fibril formation or competitive binding with ThT. This effect was less pronounced than previously observed for TauRD [27]. Among the four peptides, FibrilPaint4 showed the strongest reduction in ThT intensity (81% reduction), followed by FibrilPaint2 (58%), FibrilPaint3 (55%), and FibrilPaint1 (30%).

Next, we examined the binding of FibrilPaint peptides to HttEx1Q44 amyloid fibrils using the FibrilRuler set-up [27]. HttEx1Q44 was aggregating for 5 h, corresponding to the plateau-phase of aggregation **(Fig. 1A)**, and subsequently incubated with 200 nM FibrilPaint at a final fibril concentration of 2 µM. The hydrodynamic radius (R_h) of FibrilPaint was monitored by Flow-Induced Dispersion Analysis (FIDA) **(Fig. 1B)** [31, 32]. The average R_h of FibrilPaint1 increased from 1.7 ± 0.2 nm (free peptide) to 173 ± 44 nm in the presence of HttEx1Q44 fibrils, whereas no change was observed with monomeric HttEx1Q44. This demonstrates that FibrilPaint1 binds specifically to the fibrillar form of HttEx1Q44 but not to the monomeric protein. In contrast, FibrilPaint2–4 showed no detectable R_h increase in FIDA and were therefore ineffective in binding HttEx1Q44 fibrils **(Fig. 1B)**. This suggests that modulation of aggregation pathway is possible without strong binding. Binding specificity of FibrilPaint1 was further validated by microscale thermophoresis (MST) using fluorescently labelled FibrilPaint1 (50 nM) titrated with increasing concentrations of HttEx1Q44 fibrils or monomers (0–200 µM)

(Fig. 1C, D). MST analysis revealed a dose-dependent interaction between FibrilPaint1 and amyloid fibrils, but no measurable binding to monomers **(Fig. 1C, D)**. The apparent dissociation constant (Kd) for fibril binding was 6.0 × 10⁻□ M, calculated assuming monomer-equivalent concentrations; because each fibril comprises multiple monomeric units, the true affinity of FibrilPaint1 for the fibrillar species is likely higher. These results establish FibrilPaint1 as a unique peptide probe that selectively binds and fluorescently labels amyloid fibrils while discriminating against the monomeric form.

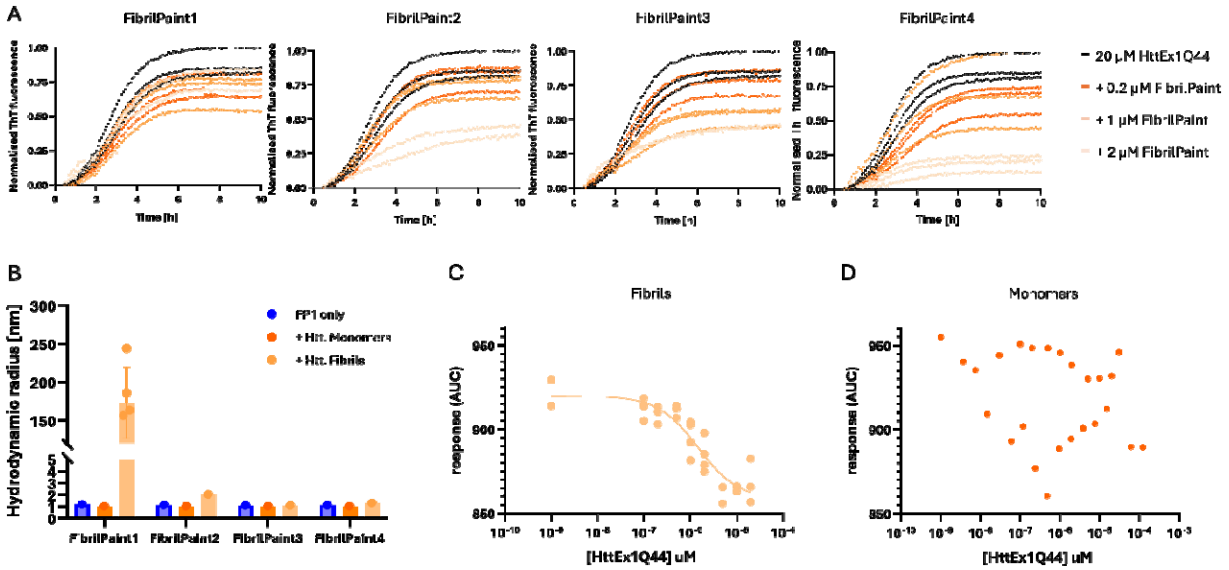

Figure 1 **FibrilPaint1 specifically binds Huntingtin Exon 1 (HttEx1Q44) amyloid fibrils. (A)** Thioflavin T (ThT) fluorescence assay showing the effect of FibrilPaint1–4 on the aggregation kinetics of 20 µM HttEx1Q44 following MBP-tag cleavage by Factor Xa (FXa). Representative graph with all triplicates shown from N=3. Fluorescence intensity is normalised to the maximum value measured at the aggregation plateau, indicating peptide-dependent reduction of the plateau value. **(B)** Hydrodynamic radius (R_h) determined by Flow-Induced Dispersion Analysis (FIDA) for FibrilPaint1–4 alone (blue), in the presence of HttEx1Q44 monomers (dark orange), or after incubation with 20 µM preformed HttEx1Q44 fibrils (light orange, 5 h aggregation). Binding to fibrils results in a pronounced R_h increase. All individual measurements shown. **(C, D)** Microscale thermophoresis (MST) analysis of 50nM FibrilPaint1 interaction with up to 150 µM HttEx1Q44 left to aggregate for 5-hours **(C)** or measured immediately (monomers) **(D)**. MST traces were recorded using a 1.5 s on-time at medium infrared power. Apparent dissociation constants (Kd ± SD) from triplicate measurements 1.6 µM for fibrils and not applicable (>10^{-4}) for monomers.

Fibril kinetics reveal continued fibril growth after ThT plateau

Next, we applied the FibrilRuler method to monitor the kinetics of HttEx1Q44 aggregation and compared its performance with conventional aggregation assays. To this end, we measured the time-dependent aggregation process in parallel using ThT

fluorescence, dynamic light scattering (DLS) for size analysis, TEM imaging and the FibrilRuler test **(Fig. 2)**. DLS determines hydrodynamic radius of particles in homogeneous solution. However, for heterogenous solutions like fibrils, it enables detection of size changes but not absolute fibril length, and rather determines the apparent hydrodynamic radius (R_h,app) [33-37].

As a benchmark, we used the ThT assay for monitoring amyloid kinetics. The ThT fluorescence profile revealed a lag phase of approximately 2 h, followed by a growth phase that reached a plateau after 5 h of aggregation, with a half-time of 3 h **(Fig. 2A)**. The control sample containing uncleaved MBP–HttEx1Q44 (without FXa) showed no increase in ThT fluorescence, confirming that aggregation was triggered by MBP cleavage. Variations in aggregation onset between replicates reflect the spontaneous and heterogeneous nature of amyloid nucleation.

In DLS measurements, monomeric MBP–HttEx1Q44 exhibited an R_h_app of 28 nm, substantially larger than the 3.5 nm predicted from its molecular weight **(Fig. 2B).** New peaks appeared to the right of the monomer peak, while the relative intensity of the monomer peak decreased **(Fig. 2B, C)**.This increased to 80 nm after 8 h of aggregation **(Fig. 2C)**. Time-resolved monitoring with DLS revealed a similar trend to that observed by ThT fluorescence during the first 4h **(Fig. 2A, D)**. R_h,app increased gradually from 0 to 4 h, after which the data seem to plateau. However, from 5h onwards, this is followed by a more pronounced rise, exceeding 80 nm at the 8 h time point. These results indicate ongoing growth of HttEx1Q44 aggregates and provides a complementary, label-free readout of fibril formation dynamics. Importantly, the monomeric peak always remained visible, indicating the cleavage is not complete at t=8h. This also means that true fibril size is likely to exceed this 80nm, as DLS provides the overall apparent value.

Next, we analysed the aggregation kinetics of HttEx1Q44 using the FibrilRuler test. In Flow-Induced Dispersion Analysis (FIDA), the diffusion of fluorescent particles is monitored as they pass through a detector; larger particles diffuse more slowly, resulting in broader peaks and an increased R_h. As an example, the peaks for t=0, t=3 and t=5h of 20 µM HttEx1Q44 aggregation are given **(Fig. 2E)**. Immediately after initiating aggregation (t = 0 h), the R_h measured for HttEx1Q44 was 1.7 nm, corresponding to the signal of free FibrilPaint. T=3 already showed a clear broadening and rightward shift of the FIDA peak, consistent with progressive formation of larger assemblies, and this trend is exceeded by timepoint t=5 **(Fig. 2E)**.

Time-resolved FibrilRuler measurements revealed a continuous increase in R_h during aggregation **(Fig. 2F)**. After 1 h, R_h reached 9.4 nm, exceeding the predicted R_h of 3.4 nm for the unfolded monomeric HttEx1Q44 structure, indicating the presence of multimeric species. Aggregation continued to increase exponentially, reaching an

average R_h of approximately 500 nm after 7 h **(Fig. 2F)**. As the particle size approached the upper limit of FIDA measurement, the final plateau value could not be determined.

Transmission electron microscopy (TEM) at 6h revealed that HttEx1Q44 fibrils began to form clusters **(Fig. 2G)**. HttEx1Q44 fibrils formed heterogeneous clusters of varying sizes, ranging from small aggregates composed of a few fibrils (50–100 nm) to large assemblies several micrometres in width. A typical clustered structure measured approximately 800 nm in length and 200 nm in width. Assuming a spherical geometry, this corresponds to an R_h of 400 nm, consistent with the 300–500 nm R_h values obtained from FIDA measurements.

Taken together, the results from ThT fluorescence, DLS, FIDA, and TEM consistently describe the aggregation of HttEx1Q44. The continued increase in size observed in both DLS and FIDA reflects progressive fibril growth and clustering, explaining the rapid and continuous rise detected by both methods. Although the general trend was apparent in DLS, measurement with FIDA captured absolute values of these clusters better. Such clustering likely does not generate additional ThT-binding sites, which explains why ThT fluorescence plateaus while FIDA and DLS continue to report increasing particle size. Together, these complementary assays demonstrate that HttEx1Q44 aggregation proceeds through the formation and coalescence of fibril clusters, leading to large assemblies that remain ThT-silent but are readily detected by hydrodynamic methods **(Fig. 2A-G)**.

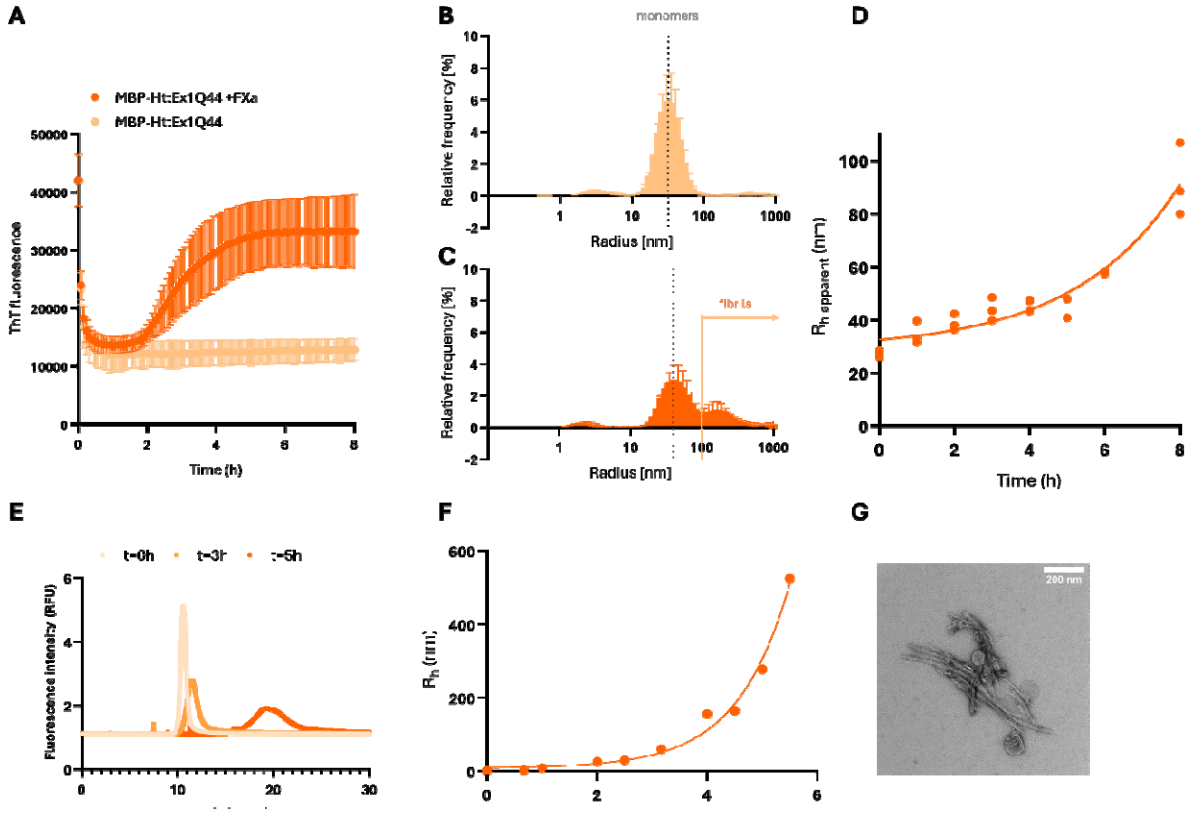

Figure 2 **Aggregation kinetics and characterization of HttEx1Q44 fibril formation. (A)** Aggregation of 20 µM HttEx1Q44 monitored by Thioflavin T (ThT) fluorescence in the presence (dark orange) or absence (light orange) of Factor Xa (FXa) for cleavage of the N-terminal MBP tag. Aggregation proceeds only after tag removal. **(B–C)** Representative Prometheus Panta measurements of the apparent hydrodynamic radius (R_h,app) of **(B)** monomeric MBP–HttEx1Q44 (28 nm) and **(C)** HttEx1Q44 fibrils after 8 h of aggregation (80 nm). **(D)** Time-resolved evolution of R_h,app during HttEx1Q44 aggregation as measured by Prometheus Panta. **(E)** Representative graphs of HttEx1Q44 samples at 0, 3, and 5 h using the FibrilRuler setup: using fluorescently labelled FibrilPaint1to label amyloids andsubsequent FIDA analysis. Shown are Progressive delay and broadening of the FIDA peaks indicate increasing particle size, reflected in a larger hydrodynamic radius (R_h) **(F)** Time-resolved evolution of R_h, during HttEx1Q44 aggregation using the FibrilRuler setup. **(G)** Transmission electron microscopy (TEM) images of HttEx1Q44 fibrils after 6 h aggregation.

FibrilPaint1 inhibits fibril clustering

Next, we analysed the effect of FibrilPaint1 when present during HttEx1Q44 aggregation, as its presence appeared to lower the ThT fluorescence plateau **(Fig. 1A)**. This reduction could result either from (1) an interaction of FibrilPaint1 with intermediate or fibrillar species, thereby altering the aggregation pathway, or (2) competition with ThT for binding sites on the fibril surface. To assess the underlying mechanism, we monitored the aggregation process using the FibrilRuler test to determine the size of the resulting assemblies.

Samples from 20 µM HttEx1Q44 aggregation reactions containing 2 µM FibrilPaint1 were collected at multiple time points and analysed by FIDA **(Fig. 3A)**. The R_h remained stable at approximately 28 nm throughout the 8 h reaction. This suggests that the presence of FibrilPaint1 inhibited further fibril growth, or continued clustering after fibril formation. Negative-stain TEM confirmed this observation, revealing that fibrils formed in the presence of FibrilPaint1 were more dispersed and exhibited less bundling compared to untreated samples **(Fig. 3B)**.

The constant R_h and the more dispersed fibril morphology observed by TEM suggest that FibrilPaint1 interacts primarily along the lateral surfaces of HttEx1Q44 fibrils. Such binding would sterically hinder fibril–fibril association, explaining the reduced bundling and lower ThT fluorescence, while allowing fibril elongation to proceed.

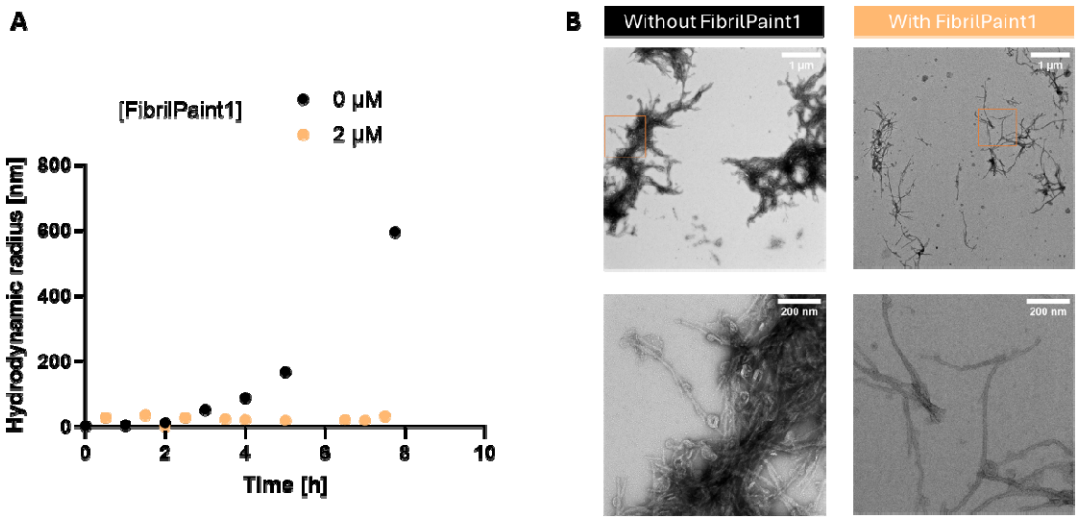

Figure 3 **FibrilPaint interacts with HttEx1Q44 fibrils during aggregation. (A)** Fibrils incubated with FibrilPaint1 were analysed using the FibrilRuler setup. The hydrodynamic radius (R_h) remained approximately 28 nm throughout the experiment (light orange). For comparison, previously acquired data of HttEx1Q44 aggregation without FibrilPaint are shown alongside (black).**(B)** Representative TEM images of HttEx1Q44 fibrils grown for 6 h without (left) or in the presence of FibrilPaint1 (right). The upper panel shows a low-magnification overview (scale bar, 1 µm), while the lower panel presents a magnified view highlighting fibril morphology (scale bar, 200 nm).

Conversion of R_h to fibril length

To better interpret the relationship between the R_h and fibril length, we analysed the properties of HttEx1Q44 layers based on previously published coordinates [12]. In this model, each layer of the fibril consists of four HttEx1Q44 monomers arranged into β-hairpins that stack to form a cross-β structure **(Fig. 4A, B)**. The flexible N- and C-terminal regions extend outward, forming a fuzzy coat. By stacking successive layers,

we established a correlation between fibril length and the number of layers, and consequently with R_h values obtained by FIDA **(Fig. 4C)**. For instance, the R_h of 9.4 nm measured after 1 h of aggregation corresponds to a structure comprising approximately 75 layers, which are roughly 300 monomers **(Fig. 2F, 4C)**. Naturally, once lateral association occurs, this simplified single-fibril model no longer applies.

After the initial layers are incorporated, fibril length approaches a linear correlation to R_h. If the 28 nm R_h measured for HttEx1Q44 in the presence of FibrilPaint1 represents unbundled fibrils, the average corresponding fibril length can be estimated 570 fibril layers, over 2000 monomers. Each layer has typical interstrand spacing for β-sheets of 0.47–0.5 nm, resulting in a length of approximately 300 nm. Thus, if the fibrils are singular, we can easily convert the R_h with the structural coordinates to the fibril length.

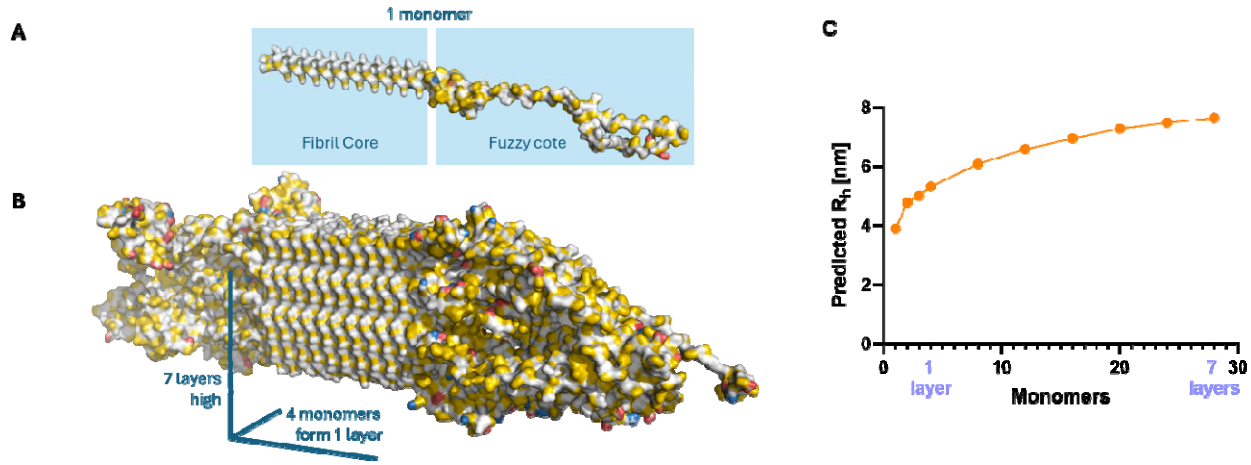

Figure 4 **Structural and mathematical representation of Huntingtin Exon 1 (HttEx1Q44) amyloid fibrils. (A)** Schematic representation of a single HttEx1Q44 monomer folded into its amyloid conformation, highlighting the ordered fibril core and the surrounding disordered fuzzy coat. **(B)** Model of a seven-layer HttEx1Q44 amyloid fibril reconstructed according to the NMR coordinates provided by the van der Well laboratory [12]. Models are coloured according to the YRB (Yellow-Red-Blue) scheme to indicate hydrophobic (yellow), negatively charged (red), and positively charged (blue) residues [38] **(C)** Mathematical correlation between the number of incorporated HttEx1Q44 monomers and predicted hydrodynamic radii (R_h) in nm. Fibril layers were generated in PyMOL and their corresponding R_h were calculated using FIDAbio software.

FibrilPaint can be used for ubiquitination, but subsequent proteasomal degradation does not occur

Having established that FibrilPaint1 interacts with HttEx1Q44 fibrils without promoting further aggregation, we next investigated whether a related peptide, FibrilPaint20 (FP20), could be used to actively modify these fibrils through ubiquitination [29]. FP20

shares the same sequence as FibrilPaint1 but lacks the fluorescent N-terminal tag. Both have an EEVD motif at the end, for targeting E3-ligase CHIP.

We first examined whether FP20 enhances the recruitment of the E3 ubiquitin ligase CHIP to HttEx1Q44 fibrils. FP20 was titrated at increasing concentrations against Atto-565–labelled CHIP (Fl-CHIP) **(Fig. 5A)**. The fluorescence baseline remained constant, indicating that binding did not alter fluorophore conformation [29]. Titration of HttEx1Q44 fibrils shows a dose-dependent increase in signal, which was enlarged in the presence of FP20, although the apparent dissociation constant (K_app) remained constant: 4.1 × 10^{-}□ M without FP20 and to 3.1 × 10^{-}□ M in its presence **(Fig. 5A)**.

Next, we evaluated ubiquitin transfer to amyloid fibrils using the complete in vitro ubiquitination cascade with FP20 as a recruiter. In the absence of ATP, the R_h was 1.8 nm, corresponding to free Fl-Ub. Upon activation of the system, the R_h increased to 62 nm for HttEx1Q44 fibrils, confirming ubiquitin conjugation **(Fig. 5B)**. After urea treatment, the R_h decreased to 45 nm, likely due partial dissociation of fibril bundles or structural heterogeneity within the HttEx1Q44 aggregates [13, 39, 40].

Next, we assessed proteasomal degradation of HttEx1Q44 fibrils using the established DLS setup (Fig. 4D, G; Fig. 5). We purified human 26S proteasomes from HEK293 GP2 cells stably expressing hRpn11-HTBH and divided them into two aliquots for immediate use. One aliquot was preincubated for 1.5 h with 50 µM of the proteasome inhibitor MG132, while the other was supplemented with buffer. Subsequently, approximately 0.2 nM of 26S proteasome was added to each sample with ubiquitinated HttEx1Q44 fibrils [41].

We incubated HttEx1Q44 fibrils with 26S proteasomes for 3.5 h in the presence or absence of MG132. To correct for variability between fibril preparations, all data were normalized to the apparent hydrodynamic radius (R_h,app) at the time of 26S addition, ensuring that subsequent changes reflected proteasomal activity rather than sample heterogeneity. In the presence of MG132, fibrils continued to grow, showing a >6-fold increase in R_h,app after 3.5 h, compared to a 4-fold increase without the inhibitor. Although the overall difference was not statistically significant, the trend was consistent across replicates. At earlier time points, Rh,app increased 1.33- and 2.6-fold at 1 h and 2 h without MG132, versus 1.20- and 3.0-fold with the inhibitor. These results suggest that proteasomal activity limits further fibril expansion under normal conditions, although effects are minimal.

Altogether, these findings show that FibrilPaint20 enables selective ubiquitination of HttEx1Q44 fibrils, while active proteasomes restrict, but do not degrade, these aggregates.

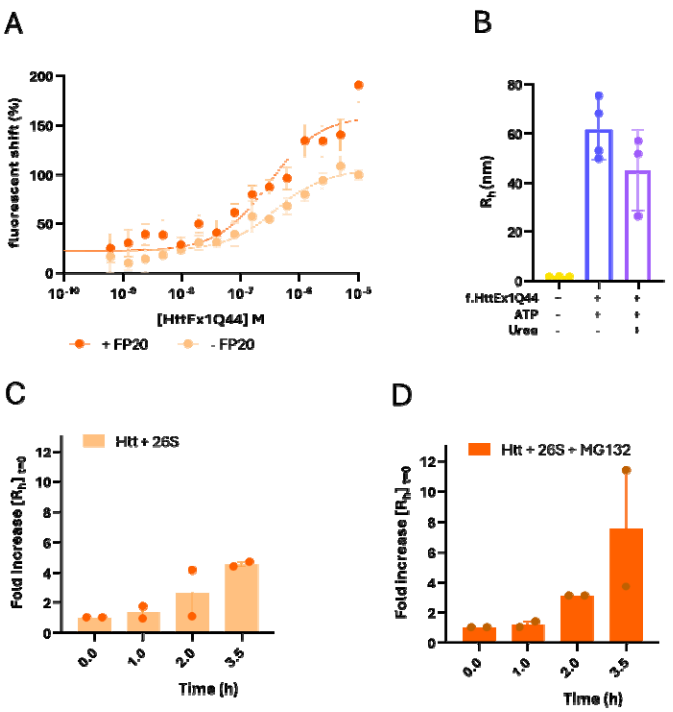

Figure 5 **Targeting HttEx1Q44 amyloid fibrils for ubiquitination with FibrilPaint20. (A)** Fluorescent shift of Atto565-labelled CHIP in presence of up to 100 µM HttEx1Q44 fibrils (light orange) measured with microscale thermophoresis. In the presence of FibrilPaint20 (FP20, dark orange), fluorescence shift increases for CHIP binding to HttEx1Q44 fibrils. Affinities are 4.1 × 10⁻□ M without FP20 and to 3.1 × 10⁻□ M in its presence. **(B)** Ubiquitin transfer assay using fluorescently labelled ubiquitin (Fl-Ub) in the complete ubiquitination cascade (E1–E2–E3) with or without ATP. In presence of ATP, the hydrodynamic radius (R_h) increases to approximately 62 nm. After urea treatment, the R_h is 45 nm, confirming covalent attachment of ubiquitin to HttEx1Q44 fibrils. **(C)** Ubiquitinated HttEx1Q44 fibrils remain stable upon addition of the 26S proteasome, indicating that ubiquitin tagging alone does not result in proteasomal degradation. **(D)** In the presence of proteasomal inhibitor MG132, fibrils display further growth.

Discussion

In this study, we establish FibrilPaint1 as a tool to investigate amyloid formation by Huntingtin Exon 1 (HttEx1). We demonstrate that FibrilPaint1 binds selectively to HttEx1 fibrils, while showing no binding with monomeric species. Using the FibrilRuler assay, we reveal fibril growth ranging from early species up to large, higher-order aggregates exceeding 600 nm in radius, resulting from processes such as fibril bundling or clustering. In parallel, we show that the non-fluorescent variant FibrilPaint20 can recruit the E3 ligase CHIP to HttEx1 amyloid fibrils, enabling ubiquitination. Together, these findings establish the FibrilPaint peptide family as both a detection platform and a modular scaffold for enzymatic modification of HttEx1 fibrils.

With the binding of FibrilPaint peptides now extended beyond tauopathies to Htt, despite the lack of sequence or structural homology, it is likely that these peptides recognise a shared structural motif across amyloid fibrils [27]. During HttEx1 aggregation, monomeric HttEx1 likely transitions from an α-helical or disordered conformation into a tetrameric intermediate by interactions between the N17 domains [14, 42, 43]. Upon formation of this nucleus, a β-sheet conformation can be established, and subsequent fibril elongation proceeds primarily as a monomer-dependent process [42, 43]. FibrilPaint1 does not inhibit HttEx1 aggregation, but reduced fibril clustering. This supports a model in which binding occurs at the sides, allowing new monomers to stack the fibrils.

Interestingly, while Tau fibrils tagged with FibrilPaint20 were efficiently ubiquitinated and degraded by the proteasome in prior work, HttEx1Q44 fibrils are not [29]. Explanations could be in the structural differences, which may affect the ability of the proteasome to cleave ubiquitinated fibrils. Clustering of HttEx1 fibrils may sterically hinder proteasomal engagement [44, 45]. The low complexity core presents uninterrupted stretches of glutamine–glutamine hydrogen bonds that pack into highly regular β-sheets, which may too densely stacked to disrupt [12, 45]. Intermediate Htt aggregates may actively impair proteasomal function by engaging the proteasome in a non-productive manner, potentially preventing gate opening or substrate translocation, and larger structures may trap the 26S proteasomes [44, 46].

Alternatively, ubiquitination levels may not be sufficient to enable proteasomal degradation of Htt fibrils. The placement of the ubiquitin group is likely on the fuzzy coat, as lysine residues are located within the N17 flanking region, which is also where patient-derived Htt fibrils are ubiquitinated [47]. Following ubiquitin recognition, the 19S regulatory subunits of the proteasome require access to an unstructured region to initiate substrate unfolding and translocation into the 20S catalytic core [48, 49]. For small fibrils, the proteasome can use these regions to pull the fibril apart [50]. For larger fibrils, the proteasome only degrades the fuzzy coat or the fibril is fragmented [51, 52]. This suggests that early and smaller fibrils may present more viable targets for proteasome-mediated clearance. Hence, it would be key for therapeutic success to start treatment at the earliest phase of the disease.

For HD, compounds like FibrilPaint could serve as tools to identify and characterize the specific amyloid species present under different physiological and pathological conditions. Misfolded Htt species capable of seeding aggregation have been detected in brain, cerebrospinal fluid, and even blood, yet their structural identity remains unknown [21, 24, 53-56]. Better molecular characterization of these species could help understand their toxicity and origin, and offers a gateway to targeted intervention. More broadly, approaches that recognize conserved amyloid structures rather than disease-specific sequences may enable a unified framework for studying protein aggregation

across neurodegenerative disorders. As disease-modifying therapies emerge, such tools will be increasingly important for linking molecular pathology to diagnosis, monitoring, and therapeutic strategy.

Acknowledgements

SGDR was supported by grants of the Campaign Team Huntington and Alzheimer Nederland (No. WE.03-2019-03) and a ZonMW TOP grant (No. 91215084). SGDR and ACOV are principal investigators of the Gravitation Consortium “FLOW” (024.006.036), funded by the Dutch Ministry of Education, Culture, and Science (OCW). FAD and SGDR were supported by NWO TakeOff1 (22073) and BioTech Booster (BIOB25014), funded by the Dutch Ministry of Education, Culture, and Science (OCW). AF thanks The Minerva Center for Bio-Hybrid complex systems and the Saerree K. and Louis P. Fiedler Chair in Chemistry. Measurements on the FIDA1, CLARIOstar® Plus and Monolith were done at the Protein Research Centre of Utrecht University**.**

Author contributions

- Conceptualization FD
- Data curation FD
- Formal analysis FD
- Funding acquisition SGDR
- Investigation FD EW
- Methodology FD
- Supervision SGDR
- Visualization FD
- Writing – original draft FD
- Writing – review and editing FD SGDR ACOV AF

Conflict of interest

FAD, AF and SGDR are named as inventors in a patent (EP23194706, ‘Peptides for the detection of amyloid fibril Aggregates’) filed by Universiteit Utrecht Holding BV describing the peptides mentioned in this manuscript. The other authors declare no competing interests.

References

[1] M. DiFiglia, E. Sapp, K.O. Chase, S.W. Davies, G.P. Bates, J.P. Vonsattel, N. Aronin, Aggregation of huntingtin in neuronal intranuclear inclusions and dystrophic neurites in brain, Science (New York, N.Y.) 277 (1997) 1990-1993.
[2] G.P. Bates, R. Dorsey, J.F. Gusella, M.R. Hayden, C. Kay, B.R. Leavitt, M. Nance, C.A. Ross, R.I. Scahill, R. Wetzel, E.J. Wild, S.J. Tabrizi, Huntington disease, Nature Reviews Disease Primers 1 (2015) 15005.
[3] A. Medina, Y. Mahjoub, L. Shaver, T. Pringsheim, Prevalence and Incidence of Huntington's Disease: An Updated Systematic Review and Meta-Analysis, Movement Disorders 37 (2022) 2327-2335.
[4] S.E. Andrew, Y.P. Goldberg, B. Kremer, H. Telenius, J. Theilmann, S. Adam, E. Starr, F. Squitieri, B. Lin, M.A. Kalchman, The relationship between trinucleotide (CAG) repeat length and clinical features of Huntington's disease, Nat. Genet. 4 (1993) 398-403.
[5] F. Saudou, S. Humbert, The Biology of Huntingtin, Neuron 89 (2016) 910-926.
[6] A.P. Lieberman, V.G. Shakkottai, R.L. Albin, Polyglutamine Repeats in Neurodegenerative Diseases, Annual Review of Pathology: Mechanisms of Disease 14 (2019) 1-27.
[7] M.E. MacDonald, C.M. Ambrose, M.P. Duyao, R.H. Myers, C. Lin, L. Srinidhi, G. Barnes, S.A. Taylor, M. James, N. Groot, A novel gene containing a trinucleotide repeat that is expanded and unstable on Huntington's disease chromosomes, Cell 72 (1993) 971-983.
[8] D.R. Langbehn, M.R. Hayden, J.S. Paulsen, P.-H.D.I.o.t.H.S.G. and the, S. Ma, I.Y. Attarwala, X.Q. Xie, CAG-repeat length and the age of onset in Huntington disease (HD): a review and validation study of statistical approaches; SQSTM1/p62: A Potential Target for Neurodegenerative Disease, ACS Chem. Neurosci. 153B; 10 (2019) 397; 2094-408; 2114.
[9] F.J. Bäuerlein, I. Saha, A. Mishra, M. Kalemanov, A. Martínez-Sánchez, R. Klein, I. Dudanova, M.S. Hipp, F.U. Hartl, W. Baumeister, In situ architecture and cellular interactions of PolyQ inclusions, Cell 171 (2017) 179-187.
[10] T.R. Peskett, F. Rau, J. O'Driscoll, R. Patani, A.R. Lowe, H.R. Saibil, A Liquid to Solid Phase Transition Underlying Pathological Huntingtin Exon1 Aggregation, Mol. Cell 70 (2018) 588-601.e6.
[11] J.G. Galaz-Montoya, S.H. Shahmoradian, K. Shen, J. Frydman, W. Chiu, Cryo-electron tomography provides topological insights into mutant huntingtin exon 1 and polyQ aggregates, Communications Biology 4 (2021) 849.
[12] M. Bagherpoor Helabad, I. Matlahov, R. Kumar, J.O. Daldrop, G. Jain, M. Weingarth, P.C.A. van der Wel, M.S. Miettinen, Integrative determination of atomic structure of mutant huntingtin exon 1 fibrils implicated in Huntington disease, Nat Commun 15 (2024) 10793.
[13] J.M. Isas, A. Langen, M.C. Isas, N.K. Pandey, A.B. Siemer, Formation and Structure of Wild Type Huntingtin Exon-1 Fibrils, Biochemistry 56 (2017) 3579-3586.
[14] C.A. Elena-Real, A. Sagar, A. Urbanek, M. Popovic, A. Morató, A. Estaña, A. Fournet, C. Doucet, X.L. Lund, Z.-D. Shi, L. Costa, A. Thureau, F. Allemand, R.E. Swenson, P.-E. Milhiet, R. Crehuet, A. Barducci, J. Cortés, D. Sinnaeve, N. Sibille, P. Bernadó, The structure of pathogenic huntingtin exon 1 defines the bases of its aggregation propensity, Nat. Struct. Mol. Biol. 30 (2023) 309-320.

[15] S.H. Scheres, M. Goedert, Molecular pathology of neurodegenerative diseases by cryo-EM of amyloids., Nature 621(7980) (2023) 701-710.
[16] S.J. Tabrizi, C. Estevez-Fraga, W.M. van Roon-Mom, M.D. Flower, R.I. Scahill, E.J. Wild, I. Muñoz-Sanjuan, C. Sampaio, A.E. Rosser, B.R. Leavitt, Potential disease-modifying therapies for Huntington's disease: lessons learned and future opportunities, The Lancet Neurology 21 (2022) 645-658.
[17] J. Saade, T.A. Mestre, Huntington's disease: latest frontiers in therapeutics, Current Neurology and Neuroscience Reports 24 (2024) 255-264.
[18] S. Ling, X. Zhang, Y. Dai, Z. Jiang, X. Zhou, S. Lu, X. Qian, J. Liu, N. Selfjord, T.M. Satir, Customizable virus-like particles deliver CRISPR–Cas9 ribonucleoprotein for effective ocular neovascular and Huntington's disease gene therapy, Nature Nanotech 20 (2025) 543-553.
[19] u. N.V., uniQure Announces Positive Topline Results from Pivotal Phase I/II Study of AMT-130 in Patients with Huntington's Disease, Lexington, Mass. and Amsterdam, 2025.
[20] S. Martí-Martínez, L.M. Valor, A Glimpse of Molecular Biomarkers in Huntington's Disease, International Journal of Molecular Sciences 23 (2022) 5411.
[21] S. Aqel, J. Ahmad, I. Saleh, A. Fathima, A.A. Al Thani, W.M. Mohamed, A.A. Shaito, Advances in Huntington's disease biomarkers: a 10-year bibliometric analysis and a comprehensive review, Biology 14 (2025) 129.
[22] J.S. Paulsen, D.K. Burks, Revised Diagnostic Criteria for Huntington Disease, Neurology Clinical Practice 15 (2025) e200430.
[23] C.M. Considine, C.M. Eddy, S.A. Frank, S.K. Kostyk, M. Oosterloo, A. Killoran, E. Furr Stimming, M. Dose, T. Cruickshank, T.D. Bird, Improving the clinical diagnostic criteria for genetically confirmed adult-onset Huntington disease: considering nonmotor presentations, Neurology: Clinical Practice 15 (2025) e200427.
[24] R.I. Scahill, M. Farag, M.J. Murphy, N.Z. Hobbs, M. Leocadi, C. Langley, H. Knights, M. Ciosi, K. Fayer, M. Nakajima, O. Thackeray, J. Gobom, J. Rönnholm, S. Weiner, Y.R. Hassan, N.K.P. Ponraj, C. Estevez-Fraga, C.S. Parker, I.B. Malone, H. Hyare, J.D. Long, A. Heslegrave, C. Sampaio, H. Zhang, T.W. Robbins, H. Zetterberg, E.J. Wild, G. Rees, J.B. Rowe, B.J. Sahakian, D.G. Monckton, D.R. Langbehn, S.J. Tabrizi, Somatic CAG repeat expansion in blood associates with biomarkers of neurodegeneration in Huntington's disease decades before clinical motor diagnosis, Nat. Med. 31 (2025) 807-818.
[25] A. Delva, M. Koole, K. Serdons, G. Bormans, L. Liu, J. Bard, V. Khetarpal, C. Dominguez, I. Munoz-Sanjuan, A. Wood, M. Skinbjerg, Y. Wang, W. Vandenberghe, K. Van Laere, Biodistribution and dosimetry in human healthy volunteers of the PET radioligands [(11)C]CHDI-00485180-R and [(11)C]CHDI-00485626, designed for quantification of cerebral aggregated mutant huntingtin, Eur. J. Nucl. Med. Mol. Imag. 50 (2022) 48-60.
[26] A. Delva, M. Koole, K. Serdons, G. Bormans, M. Skinbjerg, V. Khetarpal, L. Liu, J. Bard, R. Doot, J.H. Warner, S. Sathe, C. Sampaio, A. Wood, K. Van Laere, W. Vandenberghe, PET imaging with [^{11}C]CHDI-00485180-R, designed as radioligand for aggregated mutant huntingtin, in people with Huntington's disease, Eur. J. Nucl. Med. Mol. Imag. (2025).

[27] J. Aragonès Pedrola, F.A. Dekker, T. Garfagnini, G. Mayer, M.B. Koopman, M. Bergmeijer, G. Heesink, I. Rots, M.M.A.E. Claessens, F. Förster, J.M. Hoozemans, H. Jensen, A. Friedler, S.G.D. Rüdiger, FibrilPaint to determine the length of Tau amyloids in fluids, Proceedings of the National Academy of Sciences (2025).
[28] J. Aragonès Pedrola, F.A. Dekker, K. Guttmann, L.M. van Leeuwen, S. Singh, G. Mayer, T. Garfagnini, A. Friedler, S.G.D. Rudiger, Fibril Paint: a class of amyloid-targeting peptides, bioRxiv (2025).
[29] F.A. Dekker, J. Aragnonès Pedrola, A. den Breejen, L. Peters, A. Poza-Rodriguez, G. Mayer, S. Singh, A. Friedler, S.G.D. Rüdiger, Fibrilpaint20 directs the ubiquitin–proteasome system to Tau amyloid fibrils, BioRxiv (2025) 2024.08.27.609886.
[30] P.S. Vassar, C.F. Culling, Fluorescent stains, with special reference to amyloid and connective tissues, Archives of Pathology 68 (1959) 487-498.
[31] M.E. Pedersen, J. Østergaard, H. Jensen, Flow-Induced Dispersion Analysis (FIDA) for Protein Quantification and Characterization, in: T.M. Phillips (Ed.), Clinical Applications of Capillary Electrophoresis: Methods and Protocols, Springer New York, New York, NY, 2019, pp. 109-123.
[32] H. Jensen, J. Østergaard, Flow induced dispersion analysis quantifies noncovalent interactions in nanoliter samples, JACS 132 (2010) 4070-4071.
[33] A.M. Streets, Y. Sourigues, R.R. Kopito, R. Melki, S.R. Quake, Simultaneous measurement of amyloid fibril formation by dynamic light scattering and fluorescence reveals complex aggregation kinetics, PLoS One 8 (2013) e54541.
[34] Y. Li, V. Lubchenko, P.G. Vekilov, The use of dynamic light scattering and brownian microscopy to characterize protein aggregation, Rev. Sci. Instrum. 82 (2011) 053106.
[35] E. Velichko, S. Makarov, E. Nepomnyashchaya, G. Dong, Molecular Aggregation in Immune System Activation Studied by Dynamic Light Scattering, Biology (Basel) 9 (2020).
[36] P.A. Sokolov, V.I. Rolich, O.S. Vezo, M.V. Belousov, S.A. Bondarev, G.A. Zhouravleva, N.A. Kasyanenko, Amyloid fibril length distribution from dynamic light scattering data, Eur. Biophys. J. 51 (2022) 325-333.
[37] J. Aragonès Pedrola, M. Todorovska, S. Singh, A. Friedler, S.G.D. Rüdiger, Fibril fragmentation generates diversity in seed population, BioRxiv (2024) 2024.11.12.623277.
[38] D. Hagemans, I.A.M. van Belzen, T. Morán Luengo, S.G.D. Rüdiger, A script to highlight hydrophobicity and charge on protein surfaces, Front. Mol. Biosci. 2 (2015) 56.
[39] A. Chongtham, J.M. Isas, N.K. Pandey, A. Rawat, J.H. Yoo, T. Mastro, M.B. Kennedy, R. Langen, A. Khoshnan, Amplification of neurotoxic HTTex1 assemblies in human neurons, Neurobiology of Disease 159 (2021) 105517.
[40] J.C. Boatz, T. Piretra, A. Lasorsa, I. Matlahov, J.F. Conway, P.C.A. van der Wel, Protofilament Structure and Supramolecular Polymorphism of Aggregated Mutant Huntingtin Exon 1, J. Mol. Biol. 432 (2020) 4722-4744.
[41] X. Wang, C.-F. Chen, P.R. Baker, P.-l. Chen, P. Kaiser, L. Huang, Mass spectrometric characterization of the affinity-purified human 26S proteasome complex, Biochemistry 46 (2007) 3553-3565.
[42] A. Ceccon, V. Tugarinov, F. Torricella, G.M. Clore, Quantitative NMR analysis of the kinetics of prenucleation oligomerization and aggregation of pathogenic huntingtin exon-1 protein, Proceedings of the National Academy of Sciences 119 (2022) e2207690119.

[43] F. Torricella, V. Tugarinov, G.M. Clore, Effects of Macromolecular Cosolutes on the Kinetics of Huntingtin Aggregation Monitored by NMR Spectroscopy, The Journal of Physical Chemistry Letters 15 (2024) 6375-6382.
[44] Q. Guo, C. Lehmer, A. Martínez-Sánchez, T. Rudack, F. Beck, H. Hartmann, M. Pérez-Berlanga, F. Frottin, M.S. Hipp, F.U. Hartl, In situ structure of neuronal C9orf72 poly-GA aggregates reveals proteasome recruitment, Cell 172 (2018) 696-705. e12.
[45] D.Y. Zhao, F.J. Bäuerlein, I. Saha, F.U. Hartl, W. Baumeister, F. Wilfling, Autophagy preferentially degrades non-fibrillar polyQ aggregates, Mol. Cell 84 (2024) 1980-1994. e8.
[46] T.A. Thibaudeau, R.T. Anderson, D.M. Smith, A common mechanism of proteasome impairment by neurodegenerative disease-associated oligomers, Nat. Commun. 9 (2018) 1097-0.
[47] V. Hakim-Eshed, A. Boulos, C. Cohen-Rosenzweig, L. Yu-Taeger, T. Ziv, Y.T. Kwon, O. Riess, H.H. Phuc Nguyen, N.E. Ziv, A. Ciechanover, Site-specific ubiquitination of pathogenic huntingtin attenuates its deleterious effects, Proceedings of the National Academy of Sciences of the United States of America 117 (2020) 18661-18669.
[48] M. Mauthe, N. van de Beek, M. Mari, G. Korsten, P. Nobari, K.B. Castelino, E.P. de Mattos, I. Ouhida, J.L. Dijkstra, S. Schipper-Krom, L.R. de la Ballina, M.R. Mueller, A. Simonsen, M.S. Hipp, L.C. Kapitein, H.H. Kampinga, F. Reggiori, A chaperone-proteasome-based fragmentation machinery is essential for aggrephagy, Nat. Cell Biol. (2025).
[49] G.A. Collins, A.L. Goldberg, The Logic of the 26S Proteasome, Cell 169 (2017) 792-806.
[50] Y. Ye, D. Klenerman, D. Finley, N-Terminal Ubiquitination of Amyloidogenic Proteins Triggers Removal of Their Oligomers by the Proteasome Holoenzyme, J. Mol. Biol. 432 (2020) 585-596.
[51] R. Cliffe, J.C. Sang, F. Kundel, D. Finley, D. Klenerman, Y. Ye, Filamentous aggregates are fragmented by the proteasome holoenzyme, Cell reports 26 (2019) 2140-2149. e3.
[52] F. Parolini, E. Ataie Kachoie, G. Leo, L. Civiero, L. Bubacco, G. Arrigoni, F. Munari, M. Assfalg, M. D'Onofrio, S. Capaldi, Site-Specific Ubiquitination of Tau Amyloids Promoted by the E3 Ligase CHIP, Angew. Chem. Int. Ed. Engl. 62 (2023) e202310230.
[53] O.A. Morozova, S. Gupta, D.W. Colby, Prefibrillar huntingtin oligomers isolated from HD brain potently seed amyloid formation, FEBS Lett. 589 (2015) 1897-1903.
[54] T. Coysh, S. Mead, The future of seed amplification assays and clinical trials, Frontiers in Aging Neuroscience 14 (2022) 872629.
[55] C.Y.D. Lee, N. Wang, K. Shen, M. Stricos, P. Langfelder, K.H. Cheon, E.P. Cortés, H.V. Vinters, J.P. Vonsattel, N.S. Wexler, R. Damoiseaux, J. Frydman, X.W. Yang, Disease-related Huntingtin seeding activities in cerebrospinal fluids of Huntington’s disease patients, Scientific Reports 10 (2020) 20295.
[56] M. Rieux, M. Alpaugh, G. Sciacca, M. Saint-Pierre, M. Masnata, H.L. Denis, S.A. Lévesque, F. Herrmann, C. Bazenet, A.P. Garneau, P. Isenring, R. Truant, A. Oueslati, P.V. Gould, A. Ast, E.E. Wanker, S. Lacroix, F. Cicchetti, Shedding a new light on Huntington’s disease: how blood can both propagate and ameliorate disease pathology, Mol. Psychiatry 26 (2021) 5441-5463.